

RESEARCH ARTICLE



Functional and transcriptomic analysis of extracellular vesicles identifies calprotectin as a new prognostic marker in peripheral arterial disease (PAD)

Goren Saenz-Pipaon^{a,b}, Patxi San Martín^{c*}, Núria Planell^{d*}, Alberto Mailló^d, Susana Ravassa^{b,e,f}, Amaia Vilas-Zornoza^{c,g}, Esther Martínez-Aguilar^{b,h}, José Antonio Rodríguezⁱ, Daniel Alameda^c, David Lara-Astiaso^j, Felipe Prosper^{b,c,g,j}, José Antonio Paramo^k, Josune Orbe^l, David Gomez-Cabrero^d and Carmen Roncal^m

^aLaboratory of Atherothrombosis, Program of Cardiovascular Diseases, Cima Universidad de Navarra, Pamplona, Spain; ^bIdiSNA, Instituto de Investigación Sanitaria de Navarra, Pamplona, Spain; ^cOncohematology Program, Cima Universidad de Navarra, Pamplona, Spain; ^dTranslational Bioinformatics Unit, Navarrabiomed, Pamplona, Spain; ^eLaboratory of Heart Failure, Program of Cardiovascular Diseases, Cima Universidad de Navarra, Pamplona, Spain; ^fCIBERCV, Instituto de Salud Carlos III, Madrid, Spain; ^gCIBERONC, Instituto de Salud Carlos III, Madrid, Spain; ^hDepartamento de Angiología y Cirugía Vasculard, Complejo Hospitalario de Navarra, Pamplona, Spain; ⁱStem Cell Institute, MRC, Cambridge, UK; ^jHematology Service, Clínica Universidad de Navarra, Pamplona, Spain

ABSTRACT

Peripheral arterial disease (PAD) is associated with a high risk of cardiovascular events and death and is postulated to be a critical socioeconomic cost in the future. Extracellular vesicles (EVs) have emerged as potential candidates for new biomarker discovery related to their protein and nucleic acid cargo. In search of new prognostic and therapeutic targets in PAD, we determined the prothrombotic activity, the cellular origin and the transcriptomic profile of circulating EVs. This prospective study included control and PAD patients. Coagulation time (Procoag-PPL kit), EVs cellular origin and phosphatidylserine exposure were determined by flow cytometry in platelet-free plasma (n = 45 PAD). Transcriptomic profiles of medium/large EVs were generated using the MARS-Seq RNA-Seq protocol (n = 12/group). The serum concentration of the differentially expressed gene S100A9, in serum calprotectin (S100A8/A9), was validated by ELISA in control (n = 100) and PAD patients (n = 317). S100A9 was also determined in EVs and tissues of human atherosclerotic plaques (n = 3). Circulating EVs of PAD patients were mainly of platelet origin, predominantly Annexin V positive and were associated with the procoagulant activity of platelet-free plasma. Transcriptomic analysis of EVs identified 15 differentially expressed genes. Among them, serum calprotectin was elevated in PAD patients ($p < 0.05$) and associated with increased amputation risk before and after covariate adjustment (mean follow-up 3.6 years, $p < 0.01$). The combination of calprotectin with hs-CRP in the multivariate analysis further improved risk stratification ($p < 0.01$). Furthermore, S100A9 was also expressed in femoral plaque derived EVs and tissues. In summary, we found that PAD patients release EVs, mainly of platelet origin, highly positive for AnnexinV and rich in transcripts related to platelet biology and immune responses. Amputation risk prediction improved with calprotectin and was significantly higher when combined with hs-CRP. Our results suggest that EVs can be a promising component of liquid biopsy to identify the molecular signature of PAD patients.

ARTICLE HISTORY

Received 13 June 2019
Revised 3 February 2020
Accepted 9 February 2020

KEYWORDS

Peripheral artery disease;
extracellular vesicles;
thrombosis; RNA-Seq;
liquid-biopsy

Introduction

Peripheral arterial disease (PAD) is considered one of the most prevalent vascular conditions in developed countries, affecting more than 20% of people over 60 years of age and increasing to 50% of people older than 85. Its prevalence is estimated to increase with the ageing of the population, becoming a severe health and economic problem in the future [1]. Moreover, PAD is associated with a high occurrence of cardiovascular thrombotic events (stroke and acute myocardial

infarction) and mortality in all stages, despite the correct pharmacological control of risk factors [2]. This scenario urges us to find new therapeutic targets and prognostic tools for optimizing the diagnosis and treatment of these patients.

Extracellular vesicles (EVs) are a heterogeneous population of small membranous spheres secreted by all cell types that contain proteins, nucleic acids, lipids and sugars from the cell or organ of origin [3]. Their content depends on the particular pathophysiological condition that elicited their release at the time of

CONTACT Carmen Roncal  croncalm@unav.es  Laboratory of Atherothrombosis, Cima Universidad de Navarra, Avda. Pio XII, 55, Pamplona 31008, Spain

*These authors share second authorship.

 Supplemental data for this article can be accessed [here](#)

© 2020 The Author(s). Published by Informa UK Limited, trading as Taylor & Francis Group on behalf of The International Society for Extracellular Vesicles. This is an Open Access article distributed under the terms of the Creative Commons Attribution-NonCommercial License (<http://creativecommons.org/licenses/by-nc/4.0/>), which permits unrestricted non-commercial use, distribution, and reproduction in any medium, provided the original work is properly cited.

packaging and secretion. EVs contribute to the maintenance of vascular homeostasis by triggering responses in target cells and working as regulators of intercellular communication [3]. Classically, EVs have been described as prothrombotic agents according to their tissue factor and phosphatidylserine content [4]. Interestingly, circulating EVs also transport nucleic acids and surface markers that are considered the “molecular imprint” (liquid biopsy) of the cell or organ of origin [3]. In the cardiovascular field, EVs have emerged as potential candidates for new biomarker discovery and have been associated with the thrombophilic and inflammatory condition of coronary patients [5,6]. The role of EVs has also been investigated in PAD, although to a lesser extent, postulating their use as platelet activation markers [7–9] or as reservoirs of angiogenic and inflammatory molecules when endothelial and leukocyte-derived EVs were studied [10–12].

We hypothesized that the study of circulating EVs at functional, phenotypic and genomic levels could be a valuable tool to assess the cellular and molecular footprint of PAD patients. Therefore, we first determined the number and cellular origin of circulating EVs and their thrombotic activity. Second, we studied the transcriptome of isolated medium/large size EVs or microvesicles with an adapted massively parallel RNA sequencing (MARS-Seq) protocol and implemented a pipeline for the bioinformatics analysis of the sequencing data. Third, we measured the serum levels of one of the identified genes (S100A9, in serum calprotectin) in a large cohort of control and PAD patients to analyse its value as a prognostic marker. Finally, we determined S100A9 expression in femoral atherosclerotic plaques derived EVs and locally, in arterial tissue samples.

Methods

Baseline characteristics of PAD patients and controls

PAD patients (n = 317) were prospectively enrolled, and blood samples were collected at the time of clinical evaluation at the outpatient service of the Department of Vascular Surgery, Complejo Hospitalario de Navarra (2010–2018). Patients were classified into intermittent claudication (IC, Fontaine class II) diagnosed by haemodynamic study (Doppler ultrasound) or into critical limb ischaemia (CLI) with lower limb rest pain and/or trophic lesions (Fontaine class III–IV) confirmed by imaging studies (arteriography, magnetic resonance angiography, or ultrasonography). Exclusion criteria were as follows: previous vascular surgery, class IV patients with infected

lesions, individuals with evidence of neoplastic disease, generalized or localized inflammatory disease (moderate or severe), severe chronic kidney disease or haemodialysis, or use of anti-inflammatory drugs. The ankle brachial index (ABI) was measured at rest, as per standard technique, in the dorsalis pedis and posterior tibial arteries of both lower limbs.

A thorough medical record was assembled for all patients including cases of previous myocardial infarction, non-ischaemic cardiomyopathy, cerebrovascular disease and medication. Patients were classified as smokers (at least one cigarette daily on average over the past year), never smokers, and former smokers (no cigarette consumption in the past year). Diabetes was defined by a history of diabetes mellitus (fasting plasma glucose ≥ 126 mg/mL, or 2-h plasma glucose ≥ 200 mg/dL during oral glucose tolerance test, or A1C test $\geq 6.5\%$ [48 mol/mol]) or the use of antidiabetic drugs. Hypertension was defined by any history of hypertension or the use of antihypertensive drugs. Dyslipidaemia was defined as increased plasma concentrations of cholesterol (total-cholesterol ≥ 250 mg/mL or LDL-C ≥ 130 mg/mL) and/or triglycerides ≥ 200 mg/mL or the use of lipid-lowering drugs.

Control subjects (n = 100) were enrolled, and blood samples were collected at the time of clinical evaluation at the outpatient service of the Department of Internal Medicine, Clínica Universidad de Navarra (April 2016–December 2017). Inclusion criteria were as follows: patients older than 45 years, with ≥ 2 cardiovascular risk factors and no manifested cardiovascular disease at recruitment. Exclusion criteria included active neoplastic disease, acute or chronic inflammatory disease of any aetiology, and intake of nonsteroidal anti-inflammatory or steroid drugs 2 weeks before blood withdrawal. Samples and data from control patients included in the study were provided by the Biobank of the University of Navarra and were processed following standard operating procedures approved by the Ethical and Scientific Committees

Follow-up: PAD patients were followed up (mean average 3.6 years, min 1 month–max 8 years) to record any of the following events: amputation, ischaemic coronary disease, cerebrovascular disease and death, which was then analysed based on its origin as either all-cause mortality or cardiovascular-derived. Two major adverse cardiovascular events were defined: MACE1, including amputation and cardiovascular-death, and MACE2, including amputation and all-cause mortality.

The study was approved by the Institutional Review Boards of Complejo Hospitalario de Navarra and Clínica Universidad de Navarra,

according to the standards of the Declaration of Helsinki on medical research, and written informed consent was obtained from all patients who were enrolled in this study.

Laboratory analysis in PAD patients and controls

Serum total cholesterol, HDL cholesterol, triglycerides and glucose were measured in fasting blood samples by standard laboratory techniques. LDL cholesterol was estimated using the Friedewald equation. Plasma fibrinogen activity was measured by clotting assay (Clauss) and high-sensitivity (hs)-CRP by immunoassay (Immulite; Diagnostic Product Corporation).

Medium/large size EVs isolation from platelet-free plasma

Blood samples were drawn from the antecubital vein, with the help of a light tourniquet, by a qualified person using a butterfly device with a 21-gauge needle. Blood samples were collected in citrated tubes (VACUETTE tube 3.5 mL 9NC Coagulation sodium citrate 3.2%, Greiner Bio-one). The first few millilitres were discarded to avoid the potential artefact generated by the contact phase activation. Samples were carried from the Complejo Hospitalario de Navarra to our lab at the CIMA building (5–10 min walk) in a plastic container where tubes were unsupported. Samples were processed within 2 h after extraction. Platelet rich plasma was obtained by centrifugation (swinging bucket rotor, model SX4250, Allegra X-22 centrifuge, Beckman Coulter) at 1,800 g for 15 min at 4°C. Platelet rich plasma was collected (aspiration was stopped 1 cm above the buffy coat) and transferred into a polypropylene tube (Safe-lock 1.5 mL tube, Eppendorf) with a micropipette. Platelet rich plasma was then centrifuged (fixed angle rotor, radius 92 mm, Mikro 22R, Hettich Zentrifugen) at 14,000 g for 2 min to remove any residual platelet to obtain platelet-free plasma. Platelet-free plasma was collected into a fresh polypropylene tube using a micropipette, leaving about 20 µL of plasma at the bottom of the tube. 400 µL aliquots collected in polypropylene tubes were immediately frozen at –80°C. Haemolysed samples were excluded for EVs analysis. For medium/large size EVs isolation 400 µL platelet-free plasma was thawed at RT and centrifuged at 20,000 g for 90 min at 4°C (Mikro 22R, Hettich Zentrifugen). After removing the supernatant (platelet-free plasma residue), EVs pellet was resuspended in wash buffer (10 mM HEPES, 0.9% NaCl, pH = 7.4, filtered twice

through 0.22 µm filters) and centrifuged (Mikro 22R, Hettich Zentrifugen) at 20,000 g for 90 min at 4°C. Resulting pelleted EVs were resuspended in 50 µL wash buffer and stored at –80°C.

EVs characterization by nanoparticle tracking analysis (NTA), electron microscopy, western blot and flow cytometry

EVs particle size distribution was measured using NTA following the manufacturer's instructions (NanoSight NS300, Malvern Instruments Limited). In order to better characterize our samples, NTA was performed in the isolated EVs samples and in the platelet-free plasma residue obtained after the first 20,000 g centrifugation step (n = 3/group, Figure 2(a), and Supplemental Figure 1A and B)

To assess EVs protein markers [13], 40 µL of isolated EVs (10^9 EVs) lysed by thermal shock ($3 \times 37^\circ\text{C}$ -liquid N_2) were separated by SDS-PAGE (4–20% Mini-PROTEAN TGX Stain-Free, Bio-Rad) and transferred onto nitrocellulose membrane (iBLOT, Invitrogen, ThermoFisher). Blots were incubated overnight with primary antibodies: Alix (mouse Anti-AIP1, clone 49/AIP1, 0.125 µg/mL BD Bioscience), EMMPRIN (mouse monoclonal anti-human EMMPRIN/CD147, clone IT10C5, 1 µg/mL, Immunotools), ApoA1 (rabbit polyclonal anti-Apolipoprotein A1, sc-30089, 2 µg/mL, Santa Cruz), ApoB100 (goat polyclonal anti human Apolipoprotein B100, AF3260, 1 µg/mL, Novus Biologicals) and S100A9 (rabbit polyclonal anti-human S100A9, 0.4 µg/mL, Invitrogen) followed by 1 h incubation with required peroxidase-conjugated secondary antibodies. Peroxidase activity was detected with a chemiluminescent substrate (TMA-6, Lumigen) and images acquired with Chemidoc MP Imaging system (Bio-Rad). Loading was verified using the stain-free gel images generated with Chemidoc MP Imaging system (Bio-Rad).

Flow cytometry was performed to address carboxy-fluorescein N-succinimidyl ester (CFSE, Sigma) uptake by medium/large EVs [14] (Figure 2(d,e)). A total of 20 µL of isolated EVs (5×10^9 EVs) were stained with CFSE to a final concentration of 200 µM (from a stock of 5 mM CFSE in DMSO) for 30 min at 37°C. To remove the unbound dye 500 µL of 2% BSA in wash buffer (10 mM HEPES, 0.9% NaCl, pH = 7.4, filtered two times through 0.22 µm filters) were added and samples centrifuged 90 min at 20,000 g (Mikro 22R, Hettich Zentrifugen). The resulting pellet was diluted in 100 µL wash buffer for flow cytometry on a CytoFLEX cytometer (Beckman Coulter). The gating strategy was defined with calibrated polystyrene beads of 0.25, 0.58, 0.79 and 1.34 µm (Spherotech) using the

violet side scatter (Violet-SSC) against the regular SSC (488 nm) to trigger a signal to discriminate the noise, resulting in higher particle resolution compared to the forward side scatter (FSC). Results were analysed with CytExpert 2.1 software (Beckman Coulter).

Cryo-electron microscopy analysis of isolated EVs was performed as previously described [15]. EVs preparations were directly adsorbed onto holey-carbon support films (R 2/2 on Copper 300 mesh grids; Quantifoil). Grids were blotted with absorbent standard Vitrobot filter paper (Ø55/20 mm, Grade 595, Thermo Fisher Scientific – FEI) with the aid of a Vitrobot Mark II (FEI Company, USA) in order to create an “ultra-thin liquid film” (i.e. typically below ~300 nm film thicknesses). Grids were blotted inside the chamber of the Vitrobot at a relative humidity of 85% and at a temperature of 8°C. After blotting step, the grids were rapidly plunged into a liquid ethane bath, previously cooled with liquid nitrogen at approximately –170°C. Then, the vitrified grids were removed from the plunger and stored under liquid nitrogen inside a cryo-grid storage box. Once the samples were vitrified, they were imaged at liquid nitrogen temperature using a JEM-2200FS/CR transmission cryo-electron microscope (JEOL Europe, Croissy-sur-Seine, France) equipped with a field emission gun and operated at an acceleration voltage of 200 kV. For imaging under cryo conditions, each of the vitrified grids was cryo-transferred to a 626 DH cryo transfer holder (Gatan Inc.) and analysed at liquid nitrogen temperature (–174°C). During imaging, no-tilted zero-loss two-dimensional images were recorded under low-dose conditions, utilizing the “Minimum Dose System (MDS)” of Jeol software, with a total dose on the order of 10–20 electrons/Å² per exposure, at defocus values ranging from 1.5 to 4.0 µm. The in-column Ω energy filter of the microscope help us to record images with improved signal-to-noise ratio (SNR) by zero-loss filtering, using an energy selecting slit width of 30 eV centred at the zero-loss peak of the energy spectra. Digital images were recorded on a 4K × 4K (15 µm pixels) Ultrascan4000 charge-coupled device (CCD) camera (Gatan Inc.) using DigitalMicrograph software (Gatan Inc.), at different nominal magnifications from 15,000× to 40,000×.

EVs cellular origin by flow cytometry

Platelet-free plasma from unselected PAD patients (n = 45), obtained as indicated above, was thawed at RT and EVs labelled with FITC AnnexinV (Biolegend) and specific antibodies: PE anti-human CD62E for endothelium, (clone HCD62E, Biolegend), APC anti-human

CD41/61 for platelets (clone A2A9/6, Biolegend), PC7 anti-human CD11b (clone Bear1, Beckman Coulter) for leukocytes and PerCP/Cy5.5 anti-human CD235a for erythrocytes (clone, HI264, Biolegend). Isotype control antibodies PE mouse IgG2a,κ (clone MOPC-173, Biolegend), APC mouse IgG2a,κ (clone MOPC-173, Biolegend), PC7 mouse IgG1 (clone 679.1Mc7, Beckman Coulter), PerCP/Cy5.5 mouse IgG2a,κ (clone MOPC-173, Biolegend) were used as negative controls. Antibodies and corresponding isotype controls were diluted in binding buffer (10 mM HEPES, 150 mM NaCl, 2.5 mM CaCl₂, pH = 7.4, filtered two times through 0.22 µm filters) to achieve the working solution, and centrifuged 5 min at 13,000 rpm (Mikro 22R, Hettich Zentrifugen). The remaining supernatant containing antibodies was used for platelet-free plasma immunostaining (20 min, at RT in darkness) and posterior AnnexinV staining (1:20 final dilution, 20 min, at RT in darkness). Flow cytometry was performed on a CytoFLEX cytometer (Beckman Coulter). The gating strategy was defined with calibrated beads (Spherotech) as specified above. Results were analysed with CytExpert 2.1 software (Beckman Coulter).

Procoagulant activity of platelet-free plasma

Procoagulant phospholipid-dependent clotting time was determined with a STA Procoag-PPL kit (Stago, France) on unselected platelet-free plasma samples (n = 45 PAD) following the manufacturer’s instructions.

RNA-Seq library construction

RNA-Seq was performed in EVs (details are provided in Supplemental Methods) from controls, PAD patients with intermittent claudication (IC, Fontaine class IIa) and PAD patients with critical limb ischaemia (CLI, Fontaine class IV) with myocardial infarction in the follow-up study (n = 12/group). The protocol was adapted from Jaitin et al., 2014 (MARS-Seq) [16]. Briefly, 50 µL of isolated EVs were mixed with 50 µL of Lysis/Binding Buffer (Invitrogen). Poly-A RNA was captured with Dynabeads Oligo (dT) (Invitrogen) and reverse-transcribed with AffinityScript Multiple Temperature Reverse Transcriptase (Agilent) using oligo (dT) primers carrying a 7 bp index. Up to eight samples with similar overall RNA content were pooled together and subjected to linear amplification by in vitro transcription using a HiScribe T7 High Yield RNA Synthesis Kit (New England Biolabs). Amplified RNA was fragmented into 250–350 bp with RNA Fragmentation Reagents (Invitrogen) and dephosphorylated with thermosensitive alkaline phosphatase (FastAP, Thermo). Partial Illumina adaptor sequences

[16] were ligated with T4 RNA Ligase 1 (New England Biolabs), followed by a second reverse transcription reaction. Full Illumina adaptor sequences were added with KAPA HiFi DNA Polymerase (Kapa Biosystems). Libraries were sequenced in an Illumina NextSeq 500 at a sequence depth of 10 million reads per sample. All RNA-Seq data have been submitted to NCBI GEO repository, study number GSE140320.

Bioinformatics analysis

Single-end sequencing data quality was assessed with FastQC software [17], and Illumina adapter sequences, polyA tails, and short reads (less than 20 bp) were removed using Cutadapt R package [18]. The resulting reads were aligned to the GRCh38.p12 reference genome with STAR software [19], obtaining BAM files with uniquely aligned reads (Supplemental Table 1). Due to the high number of duplicated reads (Supplemental Table 1), de-duplication was performed with UMI-tools *dedup* function [20], using default options. Gene expression was quantified from de-duplicated BAM files using quant3p script (github.com/ctlab/quant3p) and Ensembl gene annotation (release 92). Biotype composition of the samples was analysed with NOISeq R/Bioconductor package [21]. A data driven approach was used to select the gene-filtering threshold. For the analysis, only genes with >20 counts per million (CPM) in >10 samples were selected and normalized with TMM method using EdgeR R package [22]. Differential expression analysis was performed combining two selection criteria: parametric (Limma R/Bioconductor package [23]) and non-parametric approach (Kruskal–Wallis test). Differentially expressed genes were selected if nominal *p*-value <0.01 in both differential analysis. Gene-set enrichment analysis was conducted using mdGSA R package [24], identifying gene-sets (functionally related genes) with a coordinated and significant over- or under-expression across the gene population; to this end, genes were ranked according to their differential expression statistics (*t*-statistic). Networks of the enriched gene-sets were then visualized using the Cytoscape software [25].

Gene expression analysis (RT-PCR) on isolated EVs and femoral arteries

Prior to RNA isolation, EVs underwent pre-treatment with proteinase/RNase to eliminate co-precipitated free RNA. Briefly, 20 µL of isolated EVs were incubated with 3.5 ng/µL Proteinase K (Thermo Fisher Scientific) for 10 min at 37°C. The reaction was stopped by the incubation of the mix with 17.6 µM of Proteinase K inhibitor (Merk) for 10 min at RT. Then, 1 ng/µL RNase A (Thermo Fisher Scientific) was added and samples

incubated 20 min at 37°C. The reaction was stopped by the addition of 1.5 U/µL RNaseOUT (Thermo Fisher Scientific) for 5 min at RT. Then, total RNA was extracted using TRIzol Reagent (Thermo Fisher Scientific) following the protocol for cells as specified by the manufacturer. Total RNA was reverse transcribed with random primers (Agilent) and Oligo-dT (Agilent), and the AffinityScript Multiple Temperature Reverse Transcriptase (Agilent).

RNA from frozen femoral arteries (specimens from three independent cases undergoing femoral endarterectomy, >75% stenosis) was extracted using TRIzol Reagent (Thermo Fisher Scientific) following the manufacturer's instructions. Reverse transcription was performed with 1 µg of total RNA, random primers and Moloney murine leukaemia virus reverse transcriptase (Thermo Fisher Scientific).

Full-length transcript of S100A9 was amplified by standard PCR using KAPA2G Fast HotStart ready mix following the manufacturer's instructions (Kapa Biosystems). Probes were designed to amplify the full-length transcript of S100A9 (464 bp): Forward 5'-ACGCAACATAGA GACCATCATC-3' and Reverse 5'-ACAGCCAAG ACAGTTTGACATA-3' (IDT). Amplicon length (464 bp) was then verified by 2% agarose electrophoresis.

Real-time qPCR was performed on a ViiA 7 Real-Time PCR System (Thermo Fisher Scientific) using PrimeTime qPCR gene expression assay (IDT) for S100A9 (Hs.PT.58.20989743). Data were expressed as raw Ct values. To corroborate our results in femoral arteries, expression data from carotid atherosclerotic arteries were retrieved from the NCBI GEO database (GSE28829) [26].

Western blot for S100A9 in femoral arteries

Frozen tissues (femoral endarterectomy, >75% stenosis, n = 3 independent cases) were ground into powder, homogenized (Polytron PT3000, Kinematika AG; Littau) in radioimmunoprecipitation assay (RIPA) buffer (Sigma-Aldrich) plus cOmplete protease inhibitor cocktail (Roche) and centrifuged (10 min, 13,000rpm, 4°C, Mikro 22R, Hettich Zentrifugen). Protein concentration was determined by the Bradford assay following the manufacturer's instructions (Bio-Rad Laboratories). 20 µg of total protein were loaded for western blot analysis by SDS-PAGE. The protocol is similar to the one described above for EVs samples. S100A9 was detected by the anti-S100A9 antibody (0.4 µg/mL, Invitrogen). Loading was verified using the stain-free gel image generated with Chemidoc MP Imaging system (Bio-Rad).

Isolation of EVs from femoral arteries conditioned medium

Specimens from three independent patients undergoing femoral endarterectomy (>75% stenosis) were collected in saline (0.9% NaCl, B. Braun Medical) and processed within 1 h after collection. Tissues were cut in small pieces ($\approx 10 \text{ mm}^3$) and incubated for 24 h (relative humidity 95%, 5% CO₂ at 37°C in a Steri Cycle CO₂ incubator, Thermo Scientific) in culture medium (RPMI medium 1640 [Sigma], 2 mM L-Glutamine [Gibco, ThermoFisher], 1% penicillin/streptomycin (Sigma), filtered consecutively through 0.22 and 0.1 μm filters). The volume of the culture medium was adjusted to 6 mL/gr of tissue wet weight. Twenty-four hours later, the conditioned medium was collected and centrifuged at 3,000 g for 10 min at 20°C (Swinging Bucket Rotor, Model SX4250, Allegra X-22 Centrifuge, Beckman Coulter). The supernatant was collected and immediately stored at -80°C . Two millilitre of conditioned medium were thawed at RT to isolate medium/large EVs by centrifugation (20,000 g, 70 min at 4°C, Mikro 22R, Hettich Zentrifugen). After removing the EVs-depleted conditioned medium, EVs pellets were resuspended in wash buffer (10 mM HEPES, 0.9% NaCl, pH = 7.4, filtered consecutively through 0.22 and 0.1 μm filters) and centrifuged (20,000 g, 70 min at 4°C Mikro 22R, Hettich Zentrifugen). EVs were finally resuspended in 100 μL wash buffer and stored at -80°C for further analysis. NTA analyses of conditioned medium-derived EVs and their residue ($n = 3/\text{group}$) rendered mean sizes of $209 \pm 13 \text{ nm}$ for EVs and $182 \pm 22 \text{ nm}$ for the conditioned medium residue (Supplemental Figure 4A and B).

Calprotectin (MRP8/14) determination

Serum MRP8/14 (S100A8/A9) levels were assayed by ELISA (LegendMax Human MRP8/14 [Calprotectin], BioLegend) following the manufacturer's instructions. Inter- and intra-assay coefficients of variation for the ELISAs were <8% and <3%, respectively. The minimum detectable concentration is $0.62 \pm 0.34 \text{ ng/mL}$.

Statistical analysis of clinical samples

Continuous variables are expressed as the mean \pm SD or median (interquartile range), and categorical variables are expressed as percentages. Kolmogorov–Smirnov and Shapiro–Wilks tests were used to address if distributions were Gaussian; additionally, non-Gaussian distributed variables were logarithmically transformed and Gaussianity was addressed again. Differences among three or more groups were assessed by one-way ANOVA

followed by Bonferroni's post hoc test (two conditions). Categorical variables were compared with the χ^2 test or Fisher's exact test. Associations between calprotectin and continuous variables were examined by Pearson's test. ROC curves were plotted to assess amputation for calprotectin and hs-CRP, and their cut-off values were established with the Youden Index. Patients without outcomes were censored at the date of their last follow-up. Time to the outcomes of interest was plotted using Kaplan–Meier curves for patients stratified in the diverse groups, with statistical significance assessed using the log-rank test. Hazard ratios (HRs) and their 95% CI for death (all-cause) and MACE2 were estimated using COX regression models after covariate adjustment: age, sex, diabetes mellitus, hypertension, dyslipidaemia, estimated glomerular filtration rate (eGFR) and hs-CRP [27]. Fine-Gray competing risk models were used to obtain sub-hazard ratios (SHRs) for amputation, myocardial ischaemia, stroke, cardiovascular death and MACE1, considering all-cause death and non-cardiovascular death, as required, as competing events. Due to the low number of amputation events ($n = 24$), the following basal models were considered for adjustment: model 1, sex, age; model 2, diabetes mellitus, dyslipidaemia and model 3, hypertension and estimated glomerular filtration rate (eGFR). The proportional sub-hazard and hazard assumptions were verified using Schoenfeld's residuals for each model. If violated, standard Cox or competitive risk regression analyses were extended, including time-varying covariates for each variable that did not satisfy this assumption. The additional value of the combination calprotectin and hs-CRP cut-off values for risk prediction of amputation and MACE1 was assessed with Harrell's C statistics and the continuous net reclassification index (NRI). The variance for Harrell's C estimates was calculated using the jackknife approach with the Stata package "somersd". The variances for the NRI estimates were calculated using bootstrapping (1000 resamples) with the STATA command "incrisk". Analyses were performed with STATA version 12 and SPSS version 15. All p -values are two-tailed, and statistical significance was set at $p < 0.05$.

Results

Baseline characteristics of the study populations

Demographic and clinical parameters of the control ($n = 100$) and PAD patients ($n = 317$) are shown in Table 1. PAD patients presented an increased frequency of males, half of them diabetics. Moreover, PAD patients showed decreased levels of HDL-C, and elevated concentrations of triglycerides and the inflammatory marker hs-CRP compared to controls ($p < 0.05$ for all). When

Table 1. Demographic and clinical parameters in controls (Ctrl, n = 100) and PAD patients (n = 317) before, and after classifying PAD by disease severity in intermittent claudication (IC, n = 188) and critical limb ischaemia (CLI, n = 129).

	Ctrl n = 100	PAD n = 317	p vs. Ctrl	IC n = 188	CLI n = 129	p vs. IC
<i>Demographic and clinical data</i>						
Sex (male, %)	61	88	<0.001	89	86	0.459
Age (years)	71(8)	70(11)	0.233	68(10)	73(11)	<0.001
Smokers (%)						
Never	51	19	<0.001	13	29	0.002
Current	4	33		37	28	
Former	45	48		50	43	
Diabetes mellitus (%)	36	53	0.004	38	74	<0.001
Hypertension (%)	73	75	0.725	72	78	0.231
Dyslipidemia (%)	76	67	0.108	71	62	0.084
<i>Treatment (%)</i>						
Anticoagulants	11	13	0.667	7	20	0.001
Antiplatelets	20	77	<0.001	81	70	0.033
ACE inhibitors	16	34	<0.001	33	36	0.692
ARA-2	42	27	0.003	24	30	0.212
Calcium antagonists	11	22	0.017	18	28	0.028
Vasodilators	0	6	0.247	6	7	0.685
β-Blockers	17	26	0.079	25	26	0.786
Statins	58	69	0.041	72	64	0.130
<i>Laboratory data</i>						
Total cholesterol (mg/mL)	179(44)	172(45)	0.260	184(42)	156(43)	<0.001
LDL-C (mg/dL)	99(38)	107(83)	0.317	111(76)	103(94)	0.426
HDL-C (mg/dL)	87(38)	44(15)	<0.001	48(14)	37(13)	<0.001
Triglycerides (mg/dL)	118(57)	147(83)	0.001	152(91)	141(71)	0.279
hs-CRP (mg/L) ^a	1.8(3)	4.6(10)	<0.001	3.2(4.7)	9.7(20)	<0.001

Mean (SD) is shown. ^aLogarithmically transformed variables are presented as median (Interquartile range). ACE: angiotensin-converting enzyme, ARA-2: angiotensin II receptor antagonist, LDL: low-density lipoprotein, HDL: high-density lipoprotein, hs-CRP: high-sensitivity C reactive protein.

examining PAD patients by disease severity, critical limb ischaemia (CLI) patients were older, presented an increased frequency of traditional risk factors (e.g. diabetes, increased hs-CRP), and had worse vascular function compared to intermittent claudication (ABI): 0.67 ± 0.67 IC vs. 0.39 ± 0.14 CLI, $p = 0.002$).

Procoagulant activity in PAD patients is associated with the number of platelet EVs

EVs carry cargo and, consequently, their activity greatly depends on their cellular origin and the stimulus triggering their release [4]. Thus, we characterized EVs phenotype by flow cytometry in platelet-free plasma of PAD patients (n = 45, Figure 1(a,b)). Platelet EVs were the most abundant (median [interquartile range]: 128[252] EVs/ μ L), followed by erythrocyte (63[57] EVs/ μ L), endothelial (44[40] EVs/ μ L) and leucocytes-derived EVs (15[33] EVs/ μ L). More than 85% of platelet and erythrocyte EVs were Annexin V positive, while the percentage was lower for endothelial (70%) and leucocyte EVs (40%, Figure 1(c)). Then, we determined the coagulation time of platelet-free plasma by the STA Procoag-PPL kit and assessed its association with the number of EVs by cellular origin. We found a statistically significant inverse correlation between the number of platelet-derived EVs and coagulation time ($r = -0.405$, $p = 0.007$, Figure 1(d)), but not with other EVs subpopulations (data not shown). Our data suggest that the

procoagulant activity of circulating EVs might be related to platelet derived EVs, highly positive for Annexin V.

Transcriptional analysis of EVs identifies changes associated with PAD

After the functional and phenotypic analysis of plasma EVs, we explored their mRNA cargo by performing MARS-Seq RNA-Seq analysis. The transcriptomic analyses were performed on EVs samples isolated from platelet-free plasma applying a centrifugal force of 20,000 g, which enables the enrichment of medium/large size vesicles. Figure 2 summarizes the characteristics of isolated EVs. The NTA assay presented heterogeneous polydisperse EVs populations with mean sizes of 154 ± 10 nm in control and 160 ± 8 nm in PAD patients (n = 3/group, Figure 2(a) and Supplemental Figure 1A and B). Isolated vesicles carried the EVs markers Alix and EMMPRIN and some co-precipitated contaminants such as ApoB100 and ApoA1 (Figure 2(b) and Supplemental Figure 1C). Cryo-electron microscopy studies confirmed that isolated EVs consisted of a wide variety of particles that differed in shape and electron density, although the majority of them were round shaped (Figure 2(c) and Supplemental Figure 1D). Moreover, electron dense particles lacking a visible lipid bilayer, which probably corresponded to contaminants such as VLDL or LDL, were also present in isolated EVs samples. Finally, we observed by flow cytometry that more

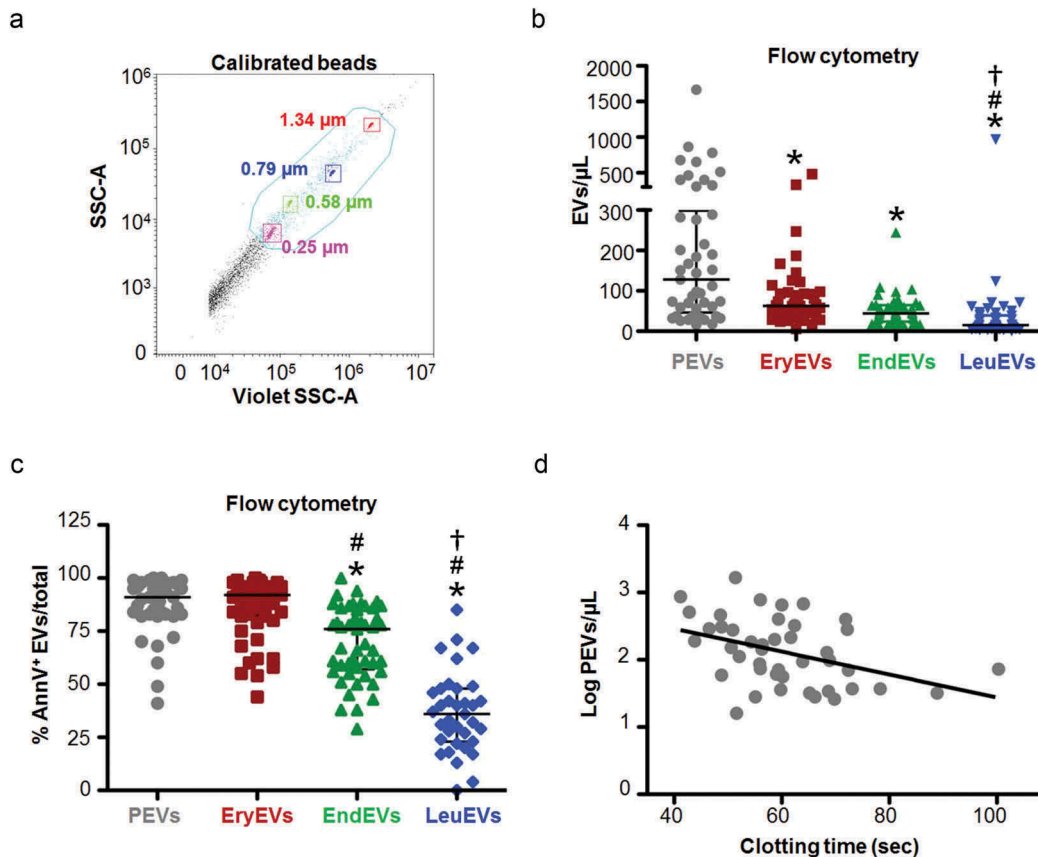


Figure 1. Platelet-derived EVs are most abundant in PAD patients. (a) Gate definition for flow cytometry analysis on platelet free-plasma using the violet side scatter (Violet-SSC) against the regular SSC. The gate was established using calibrated beads ranging from 250 nm to 1.34 μm. (b) The number and cellular origin of EVs was measured in platelet-free plasma of PAD patients by flow cytometry (n = 45). Specific antibodies for: platelets (PEVs, anti-CD41/CD61 in grey), erythrocytes (EryEVs, anti-CD235a in red), endothelial cells (EndEVs, anti-CD62E in green), and leukocytes (LeuEVs, anti-CD11b in blue) were used. Platelet derived EVs were most abundant followed by erythrocyte, endothelial and leukocyte derived EVs. Data are presented as EVs/μL. (c) Combined flow cytometry analysis for EVs cellular origin and Annexin V staining in platelet-free plasma of PAD patients. Annexin V percentage was calculated for each EVs subpopulation based on the total number of platelet, erythrocyte, endothelial and leukocyte EVs numbers respectively. (d) Correlation between the clotting time of platelet-free plasma, measured by the Procoag-PPL kit, and the number of platelet-derived EVs (PEVs, log transformed) in PAD patients (n = 43). **p* < 0.01 vs. PEVs. #*p* < 0.01 vs. EryEVs. †*p* < 0.01 vs. EndEVs.

than 80% of isolated EVs were able to uptake and process the CFSE dye (Figure 2(d,e)).

EVs of a subset of 36 selected patients were analysed (n = 12/group, Figure 3(a)): subjects without manifest vascular disease (controls, 78 ± 4 years, 58% males), and PAD patients classified by severity: intermittent claudication (IC, 72 ± 7 years, 83% males) and critical limb ischaemia (CLI, 76 ± 10 years, 92% males). Due to the highly heterogeneous RNA content in EVs, we implemented a customized bioinformatics analysis pipeline (Figure 3(a) and Supplemental Figure 2). The top 2500 most robustly expressed genes were selected for further analysis, of which, 90% were protein coding (Supplemental Table 2).

Transcriptional analysis of EVs (IC vs. control, CLI vs. control, CLI vs. IC) resulted in the robust identification of a total of 15 differentially expressed genes across patient groups (Table 2). Most of the differentially expressed genes were found altered in the CLI compared to either

control or IC groups (Figure 3(b)). Moreover, the IC group showed only five differentially expressed genes against control, suggesting that critical changes in EVs mRNA cargo might be associated with the severity of PAD patients (CLI). Hierarchical clustering and heatmap imaging revealed that most genes were upregulated in CLI patients (Figure 3(c)). Interestingly, some of the detected transcripts belonged to immune response pathways, e.g.: S100A9, LCN2, PPBP and IL16, while others were related to transcriptional regulation (AES, DNAJC8 and MED11), ubiquitination (MED11), or inactivation of MAPK activity (GPS1).

Gene Set Enrichment analysis was performed to identify up- and downregulated cellular and molecular gene-sets (such as pathways) between the studied groups (Figure 3(d)). IC patients presented an upregulation of genes related to platelet biology and immune response compared to controls (Supplemental Table 3). Likewise, an over-

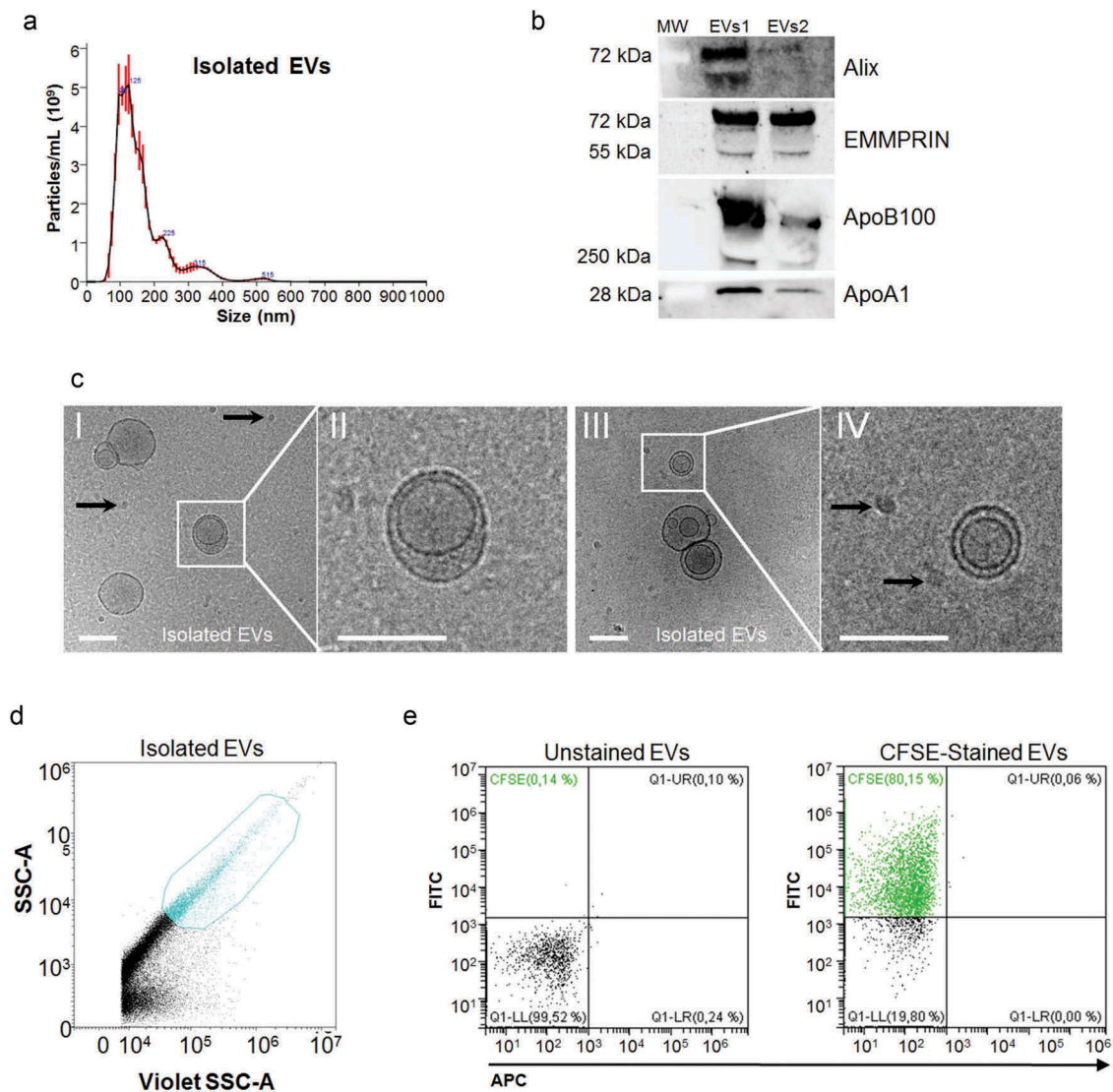


Figure 2. Characterization of isolated EVs. (a) Representative size distribution histogram for platelet-free plasma derived EVs. The NTA analysis shows a polydisperse heterogeneous vesicle population, the vast majority of them ranging from 100 to 400 nm. (b) Western blot for EVs (Alix and EMMPRIN) and non-EVs markers (ApoB100 and ApoA1) on EVs samples isolated from platelet-free plasma ($n = 2$). The first line on the left corresponds to the molecular weight marker (MW, kDa) of each detected protein. (c) Representative cryo-electron micrographs of EVs isolated from platelet-free plasma. Panels II and IV correspond to the insets drawn in panels I and III, respectively. EVs are round shaped and delimited by a lipid bilayer. Moreover, smaller electron dense particles (~ 25 nm) lacking a visible lipid membrane are observed (black arrows), indicating the presence of contaminants such as VLDL or LDL. Scale bar denotes 100 nm. (d) Representative flow cytometry dot-plot for unstained medium/large size EVs isolated from platelet-free plasma within the working gate (in blue). The gate was defined using the violet side scatter (Violet-SSC) against the regular SSC, using calibrated beads of sizes ranging from 0.25 to 1.34 μm as explained in Figure 1(a). (e) Representative dot-plots for gated EVs confronting the fluorescence intensity for FITC vs. APC. Processing of CFSE in EVs gives a positive signal in the FITC channel. Left panel shows no fluorescent signal in unstained EVs, while 80% of CFSE stained EVs are FITC positive (right panel).

representation of transcripts related to platelet biology, iron homeostasis, extracellular space and immune response were found in CLI patients vs. controls, while pathways linked to protein translation were downregulated in this comparison (Supplemental Table 4). Finally, CLI subjects presented a downregulation of pathways related to cellular translational processes compared to IC subjects (Supplemental Table 5).

Serum calprotectin levels increase in PAD patients and show significant prognostic value for amputation and MACE1

Based on the abundance of the S100A9 transcript in EVs (Table 2) and its increased expression with disease severity (Supplemental Figure 3A), S100A9 emerged as a suitable biomarker for PAD severity, and thus was

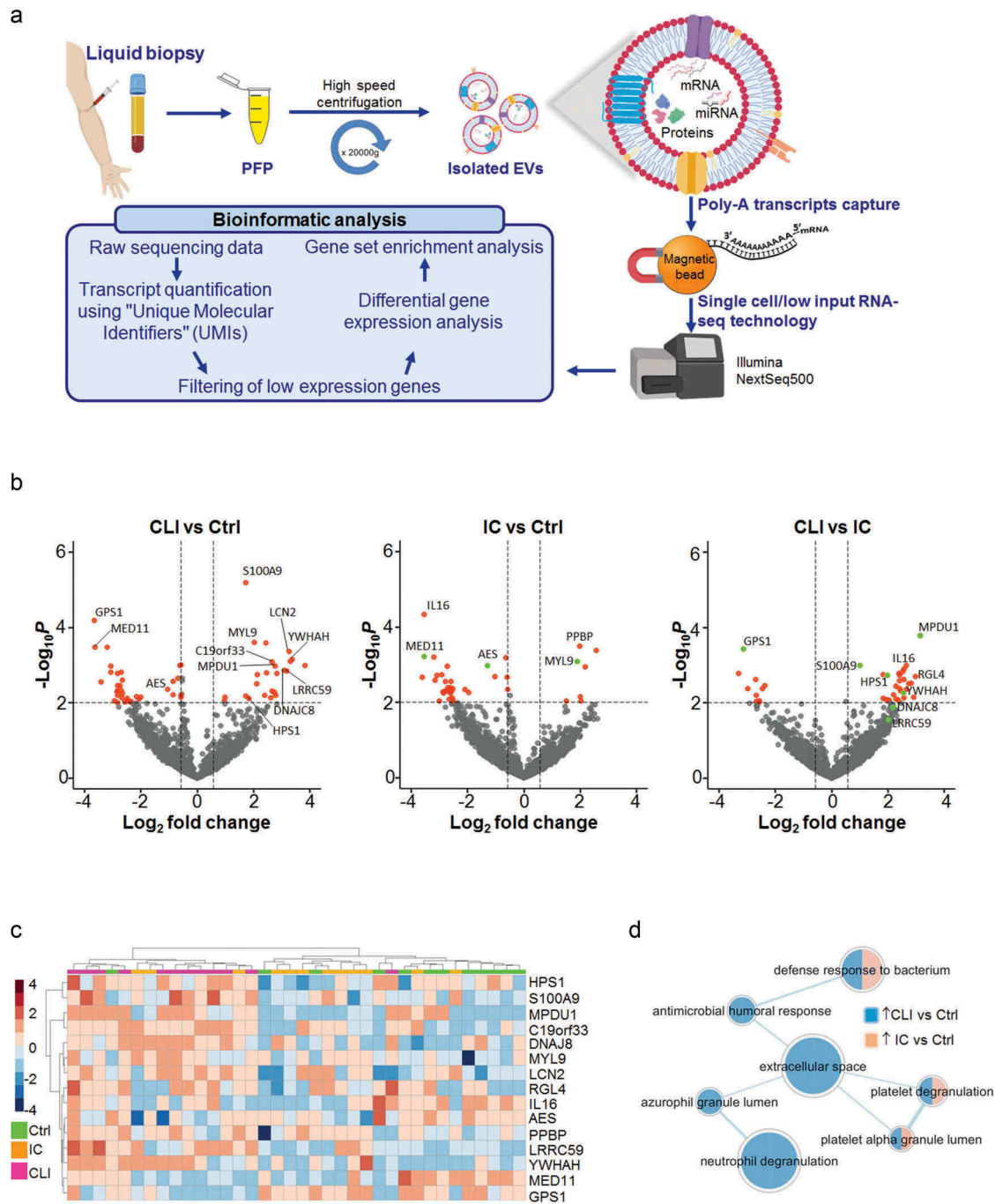


Figure 3. Downstream analysis of differential expression results in EVs. (a) Schematic overview of EVs isolation by high-speed centrifugation from platelet-free plasma. Poly-A transcripts were captured using magnetic beads and scRNA-Seq libraries were generated following an adapted protocol from Jaitin et al, [16]. Libraries were sequenced (Illumina NextSeq 500) and data questioned with an optimized bioinformatics workflow for data pre-processing and analysis. (b) Volcano plots showing the differentially expressed genes of the contrasts performed by LimmaVoom. In red, genes with a fold-change (\log_2) and p -value higher than 1.5 and 0.01, respectively. In green, genes that show differential expression in the CLI vs control contrast. (c) Hierarchical clustering (Euclidean distance) and heatmap imaging of the 15 differentially expressed genes in control and PAD patients ($n = 12/\text{group}$). Samples are arranged in columns (control in green, IC in orange and CLI in pink) and genes in rows. Up-regulated expression is shown in red and downregulated expression in blue. The heatmap was generated using counts per million expression values (CPM, logarithmically transformed) after adjustment for batch, sex and age. (d) mdGSA function enrichment network visualization by Cytoscape. Upregulated gene-sets (Gene Ontologies) for two contrasts are shown; IC vs. control in orange, and CLI vs. control in blue. Nodes size is proportional to number of genes, and edge thickness to degree of similarity between nodes.

Table 2. Differentially expressed genes after transcriptomic analysis of circulating EVs. Controls (Ctrl, n = 12), intermittent claudication (IC, n = 12) and critical limb ischaemia (CLI, n = 12).

Ensembl ID	Gene name	Fold-Change (Log2)			AveExpr (Log2-CPM)	<i>p</i>	
		IC vs. Ctrl	CLI vs. Ctrl	CLI vs. IC		Limma Voom	Kruskal–Wallis
ENSG00000104964	AES	-1.28	-1.06	0.22	9.00	0.0020	0.0023
ENSG00000129255	MPDU1	-0.39	2.76	3.16	3.65	0.0003	0.0002
ENSG00000172349	IL16	-3.54	-1.14	2.39	4.86	0.0000	0.0001
ENSG00000126698	DNAJC8	0.90	3.08	2.18	4.99	0.0023	0.0032
ENSG00000167644	C19orf33	1.48	2.65	1.17	4.65	0.0028	0.0034
ENSG00000108829	LRRCS9	1.18	3.17	1.99	3.72	0.0011	0.0044
ENSG00000163736	PPBP	1.99	0.89	-1.10	10.18	0.0009	0.0012
ENSG00000169727	GPS1	-0.53	-3.66	-3.13	5.05	0.0001	0.0001
ENSG00000161920	MED11	-3.54	-3.64	-0.10	3.70	0.0001	0.0004
ENSG00000163220	S100A9	0.70	1.71	1.01	13.43	0.0000	0.0000
ENSG00000101335	MYL9	1.89	2.03	0.13	8.16	0.0004	0.0004
ENSG00000128245	YWHAH	0.80	3.36	2.56	4.13	0.0007	0.0014
ENSG00000107521	HPS1	-0.15	1.82	1.97	5.68	0.0096	0.0034
ENSG00000159496	RGL4	-0.58	2.40	2.98	4.83	0.0022	0.0050
ENSG00000148346	LCN2	1.68	3.25	1.57	5.61	0.0009	0.0018

Genes with $p < 0.01$ obtained by LimmaVoom and Kruskal–Wallis were considered as differentially expressed. Fold changes (Log2) between the different contrasts is shown (IC vs. control; CLI vs. control; CLI vs. IC), as well as the average gene expression in all the samples (AveExpr).

selected for further studies. As a proof of concept, we confirmed the presence of the S100A9 transcript and the encoded protein in EVs isolated from platelet-free plasma by RT-qPCR, and western blot, respectively (Supplemental Figure 3B–D).

We first measured serum calprotectin in the same subjects in which the EVs RNA-Seq analysis was performed (n = 35). We observed a correlation between the levels of S100A9 mRNA in EVs, and the concentration of calprotectin in circulation ($r = 0.337$, $p = 0.048$, Figure 4(a)), suggesting that the transcriptional/protein content of EVs might also reflect changes in serum proteins.

Secondly, to determine the clinical utility of our findings, serum calprotectin was measured in the complete control and PAD cohorts (Table 1). Calprotectin expression was significantly increased in PAD (median [interquartile range]: 3.16[2.34] $\mu\text{g/mL}$ controls vs. 3.79 [3.00] $\mu\text{g/mL}$ PAD, $p = 0.007$). However, no significant differences were observed when PAD patients were classified by severity (median [interquartile range]: 3.61[2.97] $\mu\text{g/mL}$ intermittent claudication vs. 4.00 [2.88] $\mu\text{g/mL}$ critical limb ischaemia, $p = 0.052$).

Third, we assessed the prognostic value of calprotectin in PAD (mean average follow-up 3.6 years). We recorded cardiovascular events (myocardial ischaemia, n = 42 and stroke n = 26), amputation (n = 24) and mortality, either all-cause (n = 112) or cardiovascular (n = 43). MACE1 included amputation and cardiovascular-death (n = 60), and MACE2 included amputation and all-cause death (n = 121). Cox proportional hazard (HR) and sub-hazard ratios (SHR) were calculated for calprotectin, showing a significant association with amputation and MACE1 before and after covariate

adjustment (Figure 4(b,c) and Table 3), while no correlations with other cardiovascular events or death were observed (Supplemental Table 6).

Interestingly, levels of hs-CRP, a well established inflammatory marker associated with worse PAD prognosis [28], were greatly elevated in our patients (Table 1) and were also associated with amputation and MACE1 before and after covariate adjustment (Table 3). Even though, calprotectin levels seemed to better estimate risk for amputation (SHR 2.5 calprotectin vs. 1.8 hs-CRP), the correlation with MACE1 was similar for both proteins (SHR 1.5). Several authors have suggested that the combination of several biomarkers might be more accurate for cardiovascular risk prediction [28]. Therefore, we considered the possibility of improving risk evaluation by combining calprotectin and hs-CRP. ROC curves for both proteins were plotted to assess amputation risk. These analyses rendered cut-off values of ≥ 7.4 $\mu\text{g/mL}$ for calprotectin (AUC: 0.70 ± 0.06 [95% CI: 0.59–0.81], $p = 0.001$), and ≥ 13 mg/L for hs-CRP (AUC: 0.83 ± 0.03 [95% CI: 0.77–0.90], $p < 0.001$). When studied separately, high levels of calprotectin and hs-CRP increased the risk for amputation and MACE1 (Table 4). However, the best risk prediction was obtained when considering the combination of the two. Patients were divided into three groups. Group 1: low calprotectin and low hs-CRP, group 2: either high calprotectin or high hs-CRP, and group 3: high calprotectin & high hs-CRP. As shown in Table 4, amputation risk increased more than 20 times before and after covariate adjustment in group 3 and was 10-fold higher when examining MACE1 ($p < 0.001$ for all tested models). In

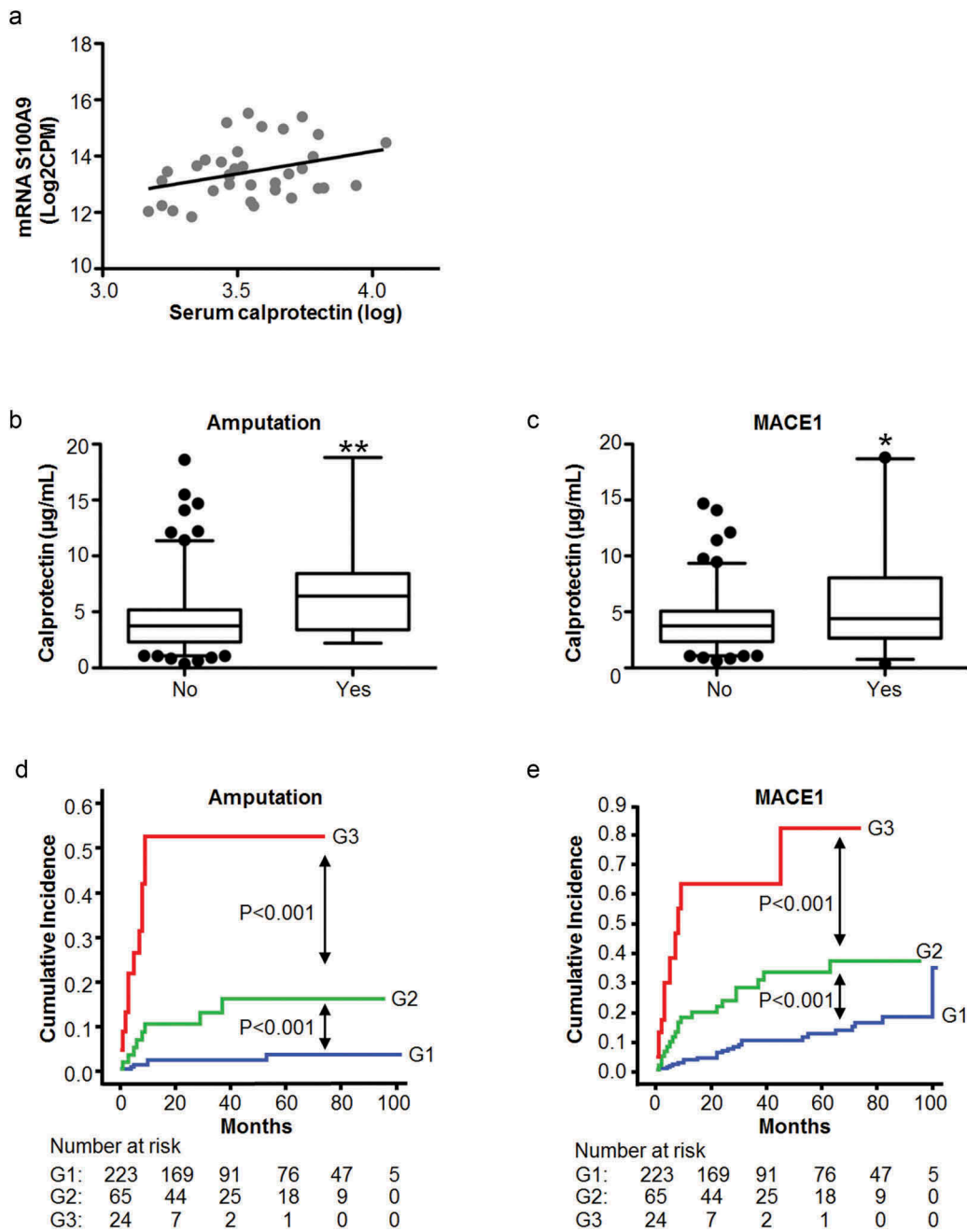


Figure 4. S100A9 mRNA expression and calprotectin levels in circulating EVs and serum of control and PAD patients. (a) The association between the mRNA levels of S100A9 in EVs measured by RNA-Seq (Y axis, log-transformed), and the serum levels of calprotectin (X axis, log-transformed) determined by ELISA in the same subjects, showed a positive significant correlation between them ($n = 35$, $r = 0.337$, $p = 0.048$). (b, c) Serum calprotectin levels were measured by ELISA in the complete PAD population ($n = 317$). Increased levels of calprotectin were observed in PAD patients with amputation (b) and MACE1 (c) in the follow-up (mean follow-up 3.6 years). $*p < 0.05$ and $**p < 0.001$ vs. no event. (d, e) Kaplan-Meier curves for the incidence of amputation (d) and MACE1 (e) in the follow-up. PAD patients were categorized according to the combination of calprotectin (≥ 7.4 µg/mL) and hs-CRP levels (≥ 13 mg/L). Group 1: low calprotectin and low hs-CRP; Group 2: either high calprotectin or high hs-CRP, and Group 3: high calprotectin & high hs-CRP. Patients with high levels of calprotectin and hs-CRP (group 3) presented increased risk for amputation and MACE1 than those within groups 1 and 2.

addition, amputation and MACE1 incidences were higher in patients from group 3 (Figure 4(d,e)).

Furthermore, to estimate the potential of the combination to improve amputation and MACE1

risk prediction, Harrell's C, IDI and NRI analyses were performed. We observed that the addition of categorized calprotectin to hs-CRP cut-off value significantly improved the accuracy of amputation

Table 3. Competing risk analyses (Fine-Gray model) for calprotectin and hs-CRP, and amputation and MACE1 in PAD patients (n = 317).

	Calprotectin ^a (µg/mL)			hs-CRP ^a (mg/L)		
	SHR	95% CI	p	SHR	95% CI	p
Amputation						
Unadjusted	2.49	1.54–4.04	<0.001	1.76	1.48–2.09	<0.001
Model 1	2.56	1.56–4.19	<0.001	1.82	1.52–2.20	<0.001
Model 2	2.62	1.58–4.34	<0.001	1.70	1.42–2.05	<0.001
Model 3	2.57	1.58–4.17	<0.001	1.74	1.47–2.07	<0.001
MACE1						
Unadjusted	1.56	1.03–2.35	0.034	1.53	1.35–1.75	<0.001
Model 1	1.70	1.14–2.54	0.009	1.48	1.28–1.70	<0.001
Model 2	1.74	1.17–2.58	0.006	1.46	1.28–1.66	<0.001

Sub-Hazard ratios (SHR) are effect sizes for a doubling of serum calprotectin and hs-CRP. Amputation models were adjusted as follows; Model 1: sex, age. Model 2: diabetes mellitus, dyslipidemia and Model 3: hypertension and estimated glomerular filtration rate (eGFR). Major adverse cardiovascular events 1 (MACE1, including amputation and CV-death) models were adjusted as follows; Model 1: sex, age. Model 2: diabetes mellitus, hypertension, dyslipidemia, eGFR. ^aLogarithmically transformed variable.

prediction (Harrell’s C AUC: 0.779 [95% CI: 0.693–0.866] vs. 0.825 [95% CI: 0.736–0.913], *p* = 0.021) and net reclassification in the unadjusted model (NRI = 0.81 [95% CI: 0.368–1.215], *p* < 0.001).

Similar results were obtained for MACE1: Harrell’s C (AUC: 0.710 [95% CI: 0.648–0.772] vs. 0.741 [95% CI: 0.675–0.807], *p* = 0.021) and net reclassification index (NRI = 0.454 [95% CI: 0.228–0.701], *p* = 0.0002). Last, we estimated outcome prediction with the combination over and beyond the basal models. The addition of the combined variable significantly increased amputation and MACE1 prediction in all tested models (Supplemental Table 7).

EVs from human atherosclerotic plaques and arterial tissues express S100A9

Finally, we studied the local expression of S100A9 in femoral atherosclerotic plaques and its presence in EVs from arterial lesions. To prove the latter, EVs were isolated from femoral atherosclerotic plaques conditioned medium by centrifugation at 20,000 g. Femoral EVs presented a mean size of 209 ± 13 nm when analysed by NTA (n = 3, Supplemental Figure 4A and B) and the expression of EVs markers Alix and

Table 4. Competing risk analyses (Fine-Gray model) for categorized calprotectin and hs-CRP, and amputation and MACE1 in PAD patients (n = 317).

	Calprotectin ≥7.4 µg/mL			hs-CRP >13 mg/L			Combination		
	SHR	95% CI	p	SHR	95% CI	p	SHR	95% CI	p
Amputation									
No Adj	7.81	3.51–17.4	<0.001	10.5	4.21–26.3	<0.001	1(ref)		
G1: Low Calp & CRP							5.42		
G2: High Calp or CRP							26.9	1.79–16.5	0.003
G3: High Calp & CRP								9.53–76.0	<0.001
Model 1	8.12	3.57–18.5	<0.001	12.0	4.58–31.1	<0.001	1(ref)		
G1: Low Calp & CRP							5.52	1.81–16.8	0.003
G2: High Calp or CRP							28.9	10.4–80.7	<0.001
G3: High Calp & CRP									
Model 2	8.22	3.68–18.3	<0.001	9.69	3.79–24.8	<0.001	1(ref)		
G1: Low Calp & CRP							5.46	1.78–16.7	0.003
G2: High Calp or CRP							25.6	8.71–75.3	<0.001
G3: High Calp & CRP									
Model 3	8.26	3.75–18.2	<0.001	11.0	4.44–27.3	<0.001	1(ref)		
G1: Low Calp & CRP							5.55	1.84–16.8	0.002
G2: High Calp or CRP							29.6	10.6–82.4	<0.001
G3: High Calp & CRP									
MACE1									
No Adj	4.13	2.32–7.34	<0.001	4.91	2.96–8.15	<0.001	1(ref)		
G1: Low Calp & CRP							2.86	1.57–5.21	0.001
G2: High Calp or CRP							12.0	6.19–23.4	<0.001
G3: High Calp & CRP									
Model 1	5.12	2.82–9.31	<0.001	4.42	2.54–7.69	<0.001	1(ref)		
G1: Low Calp & CRP							2.70	1.45–5.01	0.002
G2: High Calp or CRP							11.7	5.86–23.5	<0.001
G3: High Calp & CRP									
Model 2	5.06	2.83–9.04	<0.001	4.43	2.63–7.47	<0.001	1(ref)		
G1: Low Calp & CRP							2.90	1.63–5.18	<0.001
G2: High Calp or CRP							11.6	5.74–23.3	<0.001
G3: High Calp & CRP									

Sub-Hazard ratios (SHR). Amputation models were adjusted as follows; Model 1: sex, age. Model 2: diabetes mellitus, dyslipidemia and Model 3: hypertension and estimated glomerular filtration rate (eGFR). Major adverse cardiovascular events 1 (MACE1, including amputation and CV-death) models were adjusted as follows; Model 1: sex, age. Model 2: diabetes mellitus, hypertension, dyslipidemia, eGFR.

EMMPRIN by western blot (Supplemental Figure 4C). Cryo-electron microscopy showed round shaped EVs with a visible lipid bilayer (Supplemental Figure 4D).

The expression of S100A9 mRNA was readily detectable in EVs from femoral atherosclerotic conditioned medium by RT-qPCR (n = 3), even after treatment with proteinase K and RNase, suggesting that the transcript is carried within the EVs (Figure 5(a) and Supplemental Figure 3C, lines 5 and 6). Concomitantly, the S100A9 mRNA was also found in femoral tissue samples (qPCR, n = 3, Figure 5(a)). Additionally, public microarray data from atherosclerotic arteries (GSE28829) were interrogated showing that calprotectin was also expressed in carotid plaques (Supplemental Figure 5). The protein S100A9 was found in arterial derived EVs (n = 2, Figure 5(b)), as well as in femoral tissues (n = 3, Figure 5(c)). We detected the monomeric form of S100A9 (≈ 14 kDa), as well as bands at higher sizes (≈ 24 to 70 kDa) which might correspond

to the heterodimeric, trimeric or tetrameric forms of S100A9 as already reported by other authors [29,30].

Discussion

We report that PAD patients release EVs mainly of platelet origin and AnnexinV positive. The transcriptomic profiling of circulating EVs enabled the identification of 15 differentially expressed genes in PAD related to platelet biology and immune responses. Serum levels of one selected candidate, calprotectin (S100A8/A9 heterodimer), were elevated in PAD and associated with an increased risk of amputation and MACE1 during the follow-up. Remarkably, S100A9 mRNAs was also detected in EVs secreted from human femoral atherosclerotic plaques and tissue samples, where western blot analysis also showed S100A9 expression.

Interest in circulating EVs has grown rapidly in the cardiovascular field, as they might contain valuable

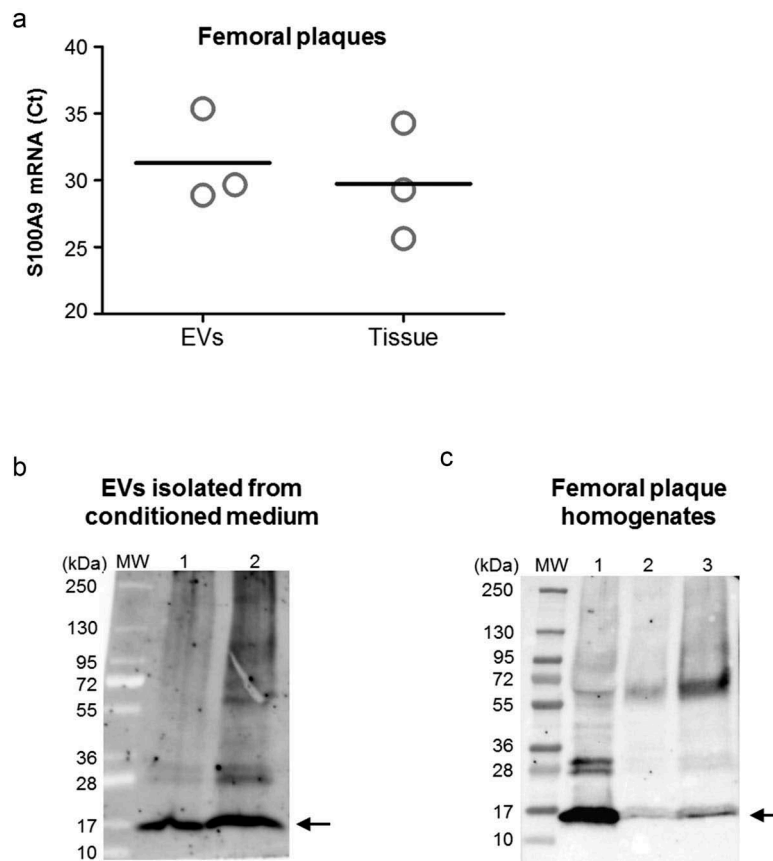


Figure 5. S100A9 expression on human femoral EVs and arterial tissue. (a) S100A9 mRNA was detected by RT-qPCR in EVs from conditioned medium of human femoral atherosclerotic plaques *ex vivo* (n = 3), and locally in femoral atherosclerotic tissues (n = 3). EVs were pretreated with proteinase K and RNase before RNA isolation to eliminate possible RNA contaminants from non-EVs sources. Data are presented as Ct values. (b, c) Representative western blots for S100A9 in EVs from femoral plaques (panel b, n = 2) and in atherosclerotic femoral tissue (panel c, n = 3). We were able to detect the monomers of S100A9 (≈ 14 kDa, black arrow), and also found bands at higher sizes (≈ 24 to 70 kDa) corresponding to the heterodimeric, trimeric or tetrameric forms of S100A9.

biological information for biomarker discovery [4]. EVs have been associated with thrombophilic and inflammatory conditions [5,6,31] and cardiovascular outcomes in coronary pathologies [6,31–33], while in PAD, they have been postulated as platelet activation markers [7]. As previously described [9,11,12], we found platelet and erythrocyte derived EVs to be the most predominant subpopulations. Interestingly, plasma coagulation time correlated with the number of platelet EVs that correspondingly displayed the highest percentage of AnnexinV staining. Our results suggest that the analysis of EVs from platelet origin might help identify PAD patients with higher prothrombotic status, although larger studies will need to be conducted to validate our hypothesis.

EVs contribute to the maintenance of vascular homeostasis by shuttling bioactive molecules from the cell or organ of origin to target cells and have been proposed to be a major component of liquid biopsy analysis in cancer and metabolic disorders [34,35]. Encapsulated into EVs, nucleic acids are protected from degradation by blood-derived RNases and facilitate the study of circulating RNAs [36]. However, the lack of methodological standardization is a major drawback for next-generation sequencing studies in EVs, starting from the election of sample-enrichment strategy, RNA-extraction protocol, library preparation, choice of multiple bioinformatics tools and, finally, data normalization technique [37]. Likewise, next-generation sequencing studies in EVs have been predominantly focused on the characterization of noncoding RNAs, mainly miRNAs, in samples enriched in exosomes [34]. Our RNA-Seq protocol was designed to pull-down 3' poly-A mRNAs [16] from samples enriched in medium/large size EVs or microvesicles, and rendered expression profiles for more than 2500 genes. By using a stringent bioinformatics workflow, that included the use of unique molecular identifiers (UMIs), we could deal with biases such as duplicated reads, thus allowing a more precise quantification of the sequenced base pairs. This way, we identified 15 differentially expressed genes in PAD associated with platelet biology and immune responses. More importantly, our results were in line with previous transcriptomic studies performed with microarrays in peripheral blood mononuclear cells [38] and femoral arteries of PAD patients [39,40]. These studies showed the upregulation of molecular pathways related to platelet biology, immune response and iron homeostasis [38–40]. Furthermore, genes involved in immune/inflammatory responses appeared to be significantly enriched according to PAD stages [39]. The number of differentially expressed genes, however, was lower in EVs compared to what has been reported previously [38–40], even if the reports were based on microarray technology [38–40], suggesting

that either the number of encapsulated transcripts is limited, the applied sequencing method lacks sensitivity for detecting low-expressed genes in EVs, or more likely, the combination of both causes the discrepancy. We should also consider that circulating EVs are a mixed population of nanospheres [3] contributing jointly to the transcriptomic profile of patients and preventing the assignation of cellular origins to the differentially expressed genes. Future studies should contemplate performing genomic analysis on discrete EVs subpopulations to establish the contribution of different cell types to PAD.

The genomic analysis of EVs might mirror systemic changes in serum proteins, and thus we determined by ELISA the circulating protein levels of one of the differentially expressed genes. Calprotectin (S100A8/A9) was selected for validation according to the relative abundance of S100A9 transcript in the RNA-Seq data. Moreover, it has shown associations with plaque instability [41,42] and cardiovascular complications in the general population [43] and in patients with acute coronary syndromes [44], while its role in PAD has been scarcely studied [45]. We determined calprotectin levels in the serum of patients included in the transcriptomic analysis and observed a linear association with S100A9 mRNA, encouraging its analysis in the expanded control and PAD populations. As previously described [45], we found increased levels of calprotectin in PAD samples, even though our control subjects were older and had at least two known cardiovascular risk factors. No significant differences were observed, however, when assessing its diagnostic potential. More interesting were the results obtained when outcome was evaluated, as current prognostic biomarkers are not completely dependable for the identification of high-risk PAD patients [1,2]. We report for the first time an association between high calprotectin levels and amputation risk, either alone or combined with cardiovascular-mortality as a composite end-point (MACE1). We performed a parallel analysis for hs-CRP levels, which are greatly increased in our population and have been proposed as a potential biomarker in PAD [46]. hs-CRP levels were independently correlated with amputation and MACE1 risk before and after covariate adjustment, although calprotectin levels seemed better suited for amputation risk evaluation when studied as a continuous variable. In line with previous reports suggesting that a multi-marker approach might be better for estimating prognosis in PAD [28], we investigated whether the combination of calprotectin and hs-CRP would improve outcome evaluation. Indeed, the greatest risk assessment was observed when expression of both proteins was elevated. We could infer from our data that; (1) calprotectin, identified after EVs transcriptomic

profiling, could improve the overall prediction of amputation in PAD either alone, or even better when combined with hs-CRP, (2) an elevated inflammatory state may contribute to the poor prognosis of PAD patients and (3) the combined measurement of inflammatory markers might be more reliable than the assessment of single biomarkers for outcome evaluation in PAD.

The genomic analysis of EVs could reflect the state of both, the vasculature and circulating cells, since all cell types, including those of the arterial wall, release EVs to the bloodstream. Here we report that EVs from femoral atherosclerotic arteries, as well as atherosclerotic plaque tissues expressed S100A9 at both mRNA and protein levels. Moreover, S100A9 expression was corroborated by interrogating public data obtained by microarray experiments in carotid plaques [26]. Thus, our data suggest that at least one of the genes identified in circulating EVs is also encapsulated by the cells of the arterial wall *ex vivo*, and expressed locally in femoral plaques. Nevertheless, no direct relationship between the genomic content of pooled EVs and the transcriptional profile of atherosclerotic plaques can be established from our study.

Limitations of the study: EVs were isolated applying a relative centrifugal force of 20,000 g, which only enriches in medium/large size EVs. In RNA-Seq experiments no treatment with proteinases/RNases was done prior to mRNA isolation, thereby we cannot exclude the presence of co-pelleted protein-shielded nucleic acids in our EVs preparations [47]. Nevertheless, we were able to detect by RT-qPCR the S100A9 transcript in EVs from platelet-free plasma and from femoral plaques after treatment with proteinase K-RNase prior to RNA isolation, suggesting that the transcript is carried within the EVs. Unique molecular identifiers (UMIs) allowed us to control PCR artefacts and more precisely quantify the sequenced reads, however 3'-UTR fragments might still be present in our samples [48], which could cause the overestimation of gene expression. Control and PAD groups differed in age and sex distribution; therefore, all bioinformatics and statistical analyses were corrected for age and sex. EVs were isolated from platelet-free plasma by centrifugation and contain different EVs subpopulations. This process could be regarded as a limitation to our study since no cellular origin could be assigned to the identified genes. Our validation cohorts could be regarded as small, but the high number of events provides the statistical power required to support our conclusions. The mean follow-up period (3.6 years) is useful to estimate short-term rather than long-term amputation risk and cardiovascular-death in PAD patients, but it is still reasonable to characterize outcomes. Since this study is a prospective analysis showing an association between calprotectin

expression levels and the risk for amputation and MACE1, no causal relationship between them can be inferred from this work. Femoral plaques for *ex vivo* EVs isolation were cut into pieces prior to incubation with culture medium. This could promote the release of intracellular materials from broken cells/tissues with densities similar to EVs (e.g.: organelles, vesicles or protein complexes) that could be co-purified in the isolation process.

Conclusions

EVs harbour proteins and nucleic acids that define their biological activity and enable the identification of potential biomarkers in cardiovascular pathologies. By combining functional, phenotypic and genomic approaches, we report that PAD patients release EVs mainly of platelet origin and highly positive for AnnexinV, thus supporting procoagulant activity. The transcriptomic analysis of EVs showed their enrichment in genes related to platelet biology and immune response. We found that circulating levels of one of those EVs-encapsulated transcripts, S100A9 (in circulation S100A8/A9 heterodimer or calprotectin), increased PAD risk prediction, further improved when combined with the established inflammatory marker hs-CRP. We propose that EVs might be a promising component for liquid biopsy analysis in PAD, enabling the discovery of new biomarkers for outcome evaluation.

Acknowledgments

We particularly acknowledge the patients for their participation, the Biobank of the University of Navarra and Dr Juan Carlos Pastrana for their collaboration. We want to thank Lara Montori for her technical assistance (Laboratory of Atherothrombosis, CIMA) and David Gil-Carton for his assistance on the cryo-electron microscopy study (CIC bioGUNE). The analysis of EVs size distribution by NTA has been performed by José-Amable Bernabe at the ICTS "NANBIOSIS", Unit 6 of the CIBER in Bioengineering, Biomaterials & Nanomedicine (CIBER-BBN) at the Barcelona Materials Science Institute.

Disclosure of interest

The authors report no conflicts of interest.

Funding

The Foundation for Applied Medical Research, Universidad de Navarra (Spain); European Fund for Economic and Regional Development (FEDER) funds [PI18/01195], Ministry of Economy and Competitiveness, Institute of

Health Carlos III [CB16/11/00371]. Patrimonio Praga (Mexico) and Virto Group (Spain).

ORCID

José Antonio Rodríguez  <http://orcid.org/0000-0002-2094-264X>

José Antonio Paramo  <http://orcid.org/0000-0003-1497-6242>

Josune Orbe  <http://orcid.org/0000-0001-6300-7670>

Carmen Roncal  <http://orcid.org/0000-0003-0616-9600>

References

- [1] Stock JK. The challenge of peripheral arterial disease: how do we improve outcome? *Atherosclerosis*. 2018;270:196–198.
- [2] Sigvant B, Lundin F, Wahlberg E. The risk of disease progression in peripheral arterial disease is higher than expected: a meta-analysis of mortality and disease progression in peripheral arterial disease. *Eur J Vasc Endovasc Surg*. 2016;51(3):395–403.
- [3] Shah R, Patel T, Freedman JE. Circulating extracellular vesicles in human disease. *N Engl J Med*. 2018;379(22):2179–2181.
- [4] Hafiane A, Daskalopoulou SS. Extracellular vesicles characteristics and emerging roles in atherosclerotic cardiovascular disease. *Metabolism*. 2018;85:213–222.
- [5] Suades R, Padró T, Crespo J, et al. Circulating micro-particle signature in coronary and peripheral blood of ST elevation myocardial infarction patients in relation to pain-to-PCI elapsed time. *Int J Cardiol*. 2016;202:378–387.
- [6] Liu Y, He Z, Zhang Y, et al. Dissimilarity of increased phosphatidylserine-positive microparticles and associated coagulation activation in acute coronary syndromes. *Coron Artery Dis*. 2016;27(5):365–375.
- [7] Zeiger F, Stephan S, Hoheisel G, et al. P-Selectin expression, platelet aggregates, and platelet-derived microparticle formation are increased in peripheral arterial disease. *Blood Coagul Fibrinolysis*. 2000;11(8):723–728.
- [8] Tan KT, Tayebjee MH, Lynd C, et al. Platelet microparticles and soluble P selectin in peripheral artery disease: relationship to extent of disease and platelet activation markers. *Ann Med*. 2005;37(1):61–66.
- [9] van der Zee PM, Biró E, Ko Y, et al. P-selectin- and CD63-exposing platelet microparticles reflect platelet activation in peripheral arterial disease and myocardial infarction. *Clin Chem*. 2006;52(4):657–664.
- [10] Vrijenhoek JE, Pasterkamp G, Moll FL, et al. Extracellular vesicle-derived CD14 is independently associated with the extent of cardiovascular disease burden in patients with manifest vascular disease. *Eur J Prev Cardiol*. 2015;22(4):451–457.
- [11] Crawford JR, Trial J, Nambi V, et al. Plasma levels of endothelial microparticles bearing monomeric C-reactive protein are increased in peripheral artery disease. *J Cardiovasc Transl Res*. 2016;9(3):184–193.
- [12] Giarretta I, Gatto I, Marcantoni M, et al. Microparticles carrying sonic hedgehog are increased in humans with peripheral artery disease. *Int J Mol Sci*. 2018;19(12):3954.
- [13] Théry C, Witwer KW, Aikawa E, et al. Minimal information for studies of extracellular vesicles 2018 (MISEV2018): a position statement of the international society for extracellular vesicles and update of the MISEV2014 guidelines. *J Extracell Vesicles*. 2018;7(1):1535750.
- [14] Morales-Kastresana A, Telford B, Musich TA, et al. Labeling extracellular vesicles for nanoscale flow cytometry. *Sci Rep*. 2017;7(1):1878.
- [15] Royo F, Gil-Carton D, Gonzalez E, et al. Differences in the metabolite composition and mechanical properties of extracellular vesicles secreted by hepatic cellular models. *J Extracell Vesicles*. 2019;8(1):1575678.
- [16] Jaitin DA, Kenigsberg E, Keren-Shaul H, et al. Massively parallel single-cell RNA-seq for marker-free decomposition of tissues into cell types. *Science*. 2014;343(6172):776–779.
- [17] Andrews S, Babraham Bioinformatics. FastQC: a quality control tool for high throughput sequence data. Manual. 2010.
- [18] Martin M. Cutadapt removes adapter sequences from high-throughput sequencing reads. *EMBnet.journal*. 2011;17(1):10.
- [19] Dobin A, Davis CA, Schlesinger F, et al. STAR: ultrafast universal RNA-seq aligner. *Bioinformatics*. 2013;29(1):15–21.
- [20] Smith T, Heger A, Sudbery I. UMI-tools: modeling sequencing errors in unique molecular identifiers to improve quantification accuracy. *Genome Res*. 2017;27(3):491–499.
- [21] Conesa A, Nueda MJ, Tarazona S, et al. Data quality aware analysis of differential expression in RNA-seq with NOISeq R/Bioc package. *Nucleic Acids Res*. 2015;43(21):e140.
- [22] Robinson MD, McCarthy DJ, Smyth GK. edgeR: a Bioconductor package for differential expression analysis of digital gene expression data. *Bioinformatics*. 2010;26(1):139–140.
- [23] Ritchie ME, Phipson B, Wu D, et al. Limma powers differential expression analyses for RNA-sequencing and microarray studies. *Nucleic Acids Res*. 2015;43(7):e47.
- [24] Montaner D, Dopazo J. Multidimensional gene set analysis of genomic data. *PLoS One*. 2010;5(4):e10348.
- [25] Merico D, Isserlin R, Bader GD. Visualizing gene-set enrichment results using the cytoscape plug-in enrichment map. In: Cagney G, Emili A. editors. *Network Biology. Methods in molecular biology (Methods and Protocols)*. Vol. 781. Clifton, NJ: Humana Press; 2011. p. 257–277. doi:10.1007/978-1-61779-276-2_12
- [26] Döring Y, Manthey HD, Drechsler M, et al. Auto-antigenic protein-DNA complexes stimulate plasmacytoid dendritic cells to promote atherosclerosis. *Circulation*. 2012;125(13):1673–1683.
- [27] Martínez-Aguilar E, Orbe J, Fernández-Montero A, et al. Reduced high-density lipoprotein cholesterol: a valuable, independent prognostic marker in peripheral arterial disease. *J Vasc Surg*. 2017;66(5):1527–1533.
- [28] Urbonaviciene G, Frystyk J, Flyvbjerg A, et al. Markers of inflammation in relation to long-term cardiovascular mortality in patients with lower-extremity peripheral arterial disease. *Int J Cardiol*. 2012;160(2):89–94.

- [29] McCormick MM, Rahimi F, Bobryshev YV, et al. S100A8 and S100A9 in human arterial wall. Implications for atherogenesis. *J Biol Chem.* 2005;280(50):41521–41529.
- [30] Hoskin TS, Crowther JM, Cheung J, et al. Oxidative cross-linking of calprotectin occurs in vivo, altering its structure and susceptibility to proteolysis. *Redox Biol.* 2019;24:101202.
- [31] Cui Y, Zheng L, Jiang M, et al. Circulating microparticles in patients with coronary heart disease and its correlation with interleukin-6 and C-reactive protein. *Mol Biol Rep.* 2013;40(11):6437–6442.
- [32] Giannopoulos G, Oudatzis G, Paterakis G, et al. Red blood cell and platelet microparticles in myocardial infarction patients treated with primary angioplasty. *Int J Cardiol.* 2014;176(1):145–150.
- [33] Vagida MS, Arakelyan A, Lebedeva AM, et al. Analysis of extracellular vesicles using magnetic nanoparticles in blood of patients with acute coronary syndrome. *Biochem (Mosc).* 2016;81(4):382–391.
- [34] Liu T, Zhang Q, Zhang J, et al. EVmiRNA: a database of miRNA profiling in extracellular vesicles. *Nucleic Acids Res.* 2019;47(D1):D89–D93.
- [35] La Marca V, Fierabracci A. Insights into the diagnostic potential of extracellular vesicles and their miRNA Signature from liquid biopsy as early biomarkers of diabetic micro/macrovacular complications. *Int J Mol Sci.* 2017;18(9):1974.
- [36] Cheng L, Sharples RA, Scicluna BJ, et al. Exosomes provide a protective and enriched source of miRNA for biomarker profiling compared to intracellular and cell-free blood. *J Extracell Vesicles.* 2014;3(1):23743.
- [37] Kuhlmann JD, Chebouti I, Kimmig R, et al. Extracellular vesicle-associated miRNAs in ovarian cancer – design of an integrated NGS-based workflow for the identification of blood-based biomarkers for platinum-resistance. *Clin Chem Lab Med.* 2019;57(7):1053–1062.
- [38] Masud R, Shameer K, Dhar A, et al. Gene expression profiling of peripheral blood mononuclear cells in the setting of peripheral arterial disease. *J Clin Bioinforma.* 2012;2(1):6.
- [39] Fu S, Zhao H, Shi J, et al. Peripheral arterial occlusive disease: global gene expression analyses suggest a major role for immune and inflammatory responses. *BMC Genomics.* 2008;9(1):369.
- [40] Croner RS, Balzer K, Schellerer V, et al. Molecular characterization of peripheral arterial disease in proximal extremity arteries. *J Surg Res.* 2012;178(2):1046–1058.
- [41] Miyamoto S, Ueda M, Ikemoto M, et al. Increased serum levels and expression of S100A8/A9 complex in infiltrated neutrophils in atherosclerotic plaque of unstable angina. *Heart.* 2008;94(8):1002–1007.
- [42] Ionita MG, Vink A, Dijke IE, et al. High levels of myeloid-related protein 14 in human atherosclerotic plaques correlate with the characteristics of rupture-prone lesions. *Arterioscler Thromb Vasc Biol.* 2009;29(8):1220–1227.
- [43] Kunutsor SK, Flores-Guerrero JL, Kieneker LM, et al. Plasma calprotectin and risk of cardiovascular disease: findings from the PREVEND prospective cohort study. *Atherosclerosis.* 2018;275:205–213.
- [44] Morrow DA, Wang Y, Croce K, et al. Myeloid-related protein 8/14 and the risk of cardiovascular death or myocardial infarction after an acute coronary syndrome in the pravastatin or atorvastatin evaluation and infection therapy: thrombolysis in myocardial infarction (PROVE IT-TIMI 22) trial. *Am Heart J.* 2008;155(1):49–55.
- [45] Engelberger RP, Limacher A, Kucher N, et al. Biological variation of established and novel biomarkers for atherosclerosis: results from a prospective, parallel-group cohort study. *Clin Chim Acta.* 2015;447:16–22.
- [46] Singh TP, Morris DR, Smith S, et al. Systematic review and meta-analysis of the association between C-reactive protein and major cardiovascular events in patients with peripheral artery disease. *Eur J Vasc Endovasc Surg.* 2017;54(2):220–233.
- [47] Mateescu B, Kowal EJK, van Balkom BWM, et al. Obstacles and opportunities in the functional analysis of extracellular vesicle RNA – an ISEV position paper. *J Extracell Vesicles.* 2017;6(1):1286095.
- [48] Batagov AO, Kurochkin IV. Exosomes secreted by human cells transport largely mRNA fragments that are enriched in the 3'-untranslated regions. *Biol Direct.* 2013;8(1):12.